Acta Pharmaceutica Sinica B 2022;12(1):228–245

Chinese Pharmaceutical Association
Institute of Materia Medica, Chinese Academy of Medical Sciences

Acta Pharmaceutica Sinica B

www.elsevier.com/locate/apsb
www.sciencedirect.com

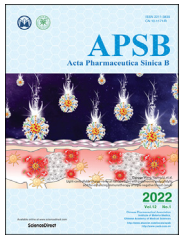

ORIGINAL ARTICLE

Targeting PDE4 as a promising therapeutic strategy in chronic ulcerative colitis through modulating mucosal homeostasis

Heng Li[a,b,†], Yao Zhang[c,†], Moting Liu[a,b], Chen Fan[a], Chunlan Feng[a], Qiukai Lu[a,b], Caigui Xiang[a,b], Huimin Lu[a,b], Xiaoqian Yang[a], Bing Wu[a,b], Duowu Zou[c,*], Wei Tang[a,b,*]

[a]*Laboratory of Anti-inflammation and Immunopharmacology, Shanghai Institute of Materia Medica, Chinese Academy of Sciences, Shanghai 201203, China*
[b]*School of Pharmacy, University of Chinese Academy of Sciences, Beijing 100049, China*
[c]*Department of Gastroenterology, Ruijin Hospital Affiliated to Shanghai Jiao Tong University School of Medicine, Shanghai 200025, China*

Received 15 February 2021; received in revised form 9 March 2021; accepted 17 March 2021

KEY WORDS

Ulcerative colitis;
PDE4;
Mucosal homeostasis;
Gut microbiota;
Epithelial barrier

Abstract Phosphodiesterase-4 (PDE4) functions as a catalyzing enzyme targeting hydrolyzation of intracellular cyclic adenosine monophosphate (cAMP) and inhibition of PDE4 has been proven to be a competitive strategy for dermatological and pulmonary inflammation. However, the pathological role of PDE4 and the therapeutic feasibility of PDE4 inhibitors in chronic ulcerative colitis (UC) are less clearly understood. This study introduced apremilast, a breakthrough in discovery of PDE4 inhibitors, to explore the therapeutic capacity in dextran sulfate sodium (DSS)-induced experimental murine chronic UC. In the inflamed tissues, overexpression of PDE4 isoforms and defective cAMP-mediating pathway were firstly identified in chronic UC patients. Therapeutically, inhibition of PDE4 by apremilast modulated cAMP-predominant protein kinase A (PKA)–cAMP-response element binding protein (CREB) signaling and ameliorated the clinical symptoms of chronic UC, as evidenced by improvements on mucosal ulcerations, tissue fibrosis, and inflammatory infiltrations. Consequently, apremilast maintained a normal intestinal physical and chemical barrier function and rebuilt the mucosal homeostasis by interfering with the cross-talk between human epithelial cells and immune cells. Furthermore, we found that apremilast could remap the landscape of gut microbiota and exert regulatory effects on antimicrobial responses and the function of mucus in the gut microenvironment. Taken together, the present study

*Corresponding authors.
E-mail addresses: zdw12125@rjh.com.cn (Duowu Zou), tangwei@simm.ac.cn (Wei Tang).
[†]These authors made equal contributions to this work.
Peer review under responsibility of Chinese Pharmaceutical Association and Institute of Materia Medica, Chinese Academy of Medical Sciences.

https://doi.org/10.1016/j.apsb.2021.04.007

revealed that intervene of PDE4 provided an infusive therapeutic strategy for patients with chronic and relapsing UC.

1. Introduction

Phosphodiesterase-4 (PDE4) functions as an infusive and competitive target in several inflammatory disorders, including asthma, psoriasis, psoriatic arthritis, allergic dermatitis, and chronic obstructive pulmonary disease[1,2]. Increased activity of PDE4 leads to overproduction of proinflammatory cytokines and chemokines in several inflammatory cells and epithelial cells, which contribute to further activation and infiltration of immune cells in the inflamed tissues[3]. Inhibition of PDE4 is well-defined to accumulate the intracellular level of cyclic adenosine monophosphate (cAMP), a critical downregulatory signal in suppressing the production of interferon-γ (IFN-γ), tumor necrosis factor-α (TNF-α), interleukin-17 (IL-17), and promoting the synthesis of IL-10[4,5]. Given the anti-inflammatory properties of PDE4 inhibitors, up to now, roflumilast, apremilast, and crisaborole have been approved by U.S. Food and Drug Administration (FDA) for attenuating bronchial and dermatological disorders[1]. Whereas, the pathological role of PDE4 and the efficacy of PDE4 inhibition in chronic ulcerative colitis (UC) need to be fully understood.

The intestinal tract is a physiological symbiotic system consisting of epithelium, mucus layer, resident microbiota, and immune cells, which facilitate tolerance of mucosal immunity, nutrient recycling, and defense function[6,7]. Chronic and relapsing UC is characterized by ulcerations, diarrhea, hematochezia, abnormal pain, and emaciation, which are linked with complicated and multilevel interactions between disturbance of mucosal immune homeostasis, dysfunction of colonic epithelial barrier, and genetic susceptibility[8,9]. Under pathological conditions, the intestinal epithelial cells and other functional cells, including goblet cells and intestinal secretory cells, are intended to undergo apoptosis or necrosis in the presence of excessive damage associated molecular patterns (DAMPs) and pathogen associated molecular patterns (PAMPs)[10]. Meanwhile, macrophages, dendritic cells (DCs), and neutrophils in the lamina propria (LP) of intestinal anatomical positions significantly expand and are activated upon Toll-like receptors[11,12]. Additionally, innate lymphoid cells (ILCs), the novel cell types in modulating mucosal inflammation, are enriched in intestinal mucosa and play an essential role in responding to microbial and environmental stimuli[13,14]. As a consequence, overexpression of inflammatory cytokines and chemokines further promote the recruitment of innate immune cells, T helper cells, natural killer (NK) cells, and other hematopoietic cells from peripheral circulatory system or lymphatic vessels, which collectively lead to outbreak of tissue damage and inflammation in UC[12,15,16].

Humans and microbes have coexisted for a long time and live in a beneficial symbiotic association during evolution and maintaining the homeostasis of the gut microenvironment. Whereas, the microbiome manifests as a fragile balance and deranged communication between host and microorganism is thought to provoke the immune system and increase the permeability of intestinal epithelial barrier in the development of UC[17,18]. In the previous research, the population of probiotics, which promote nutrients absorption and improve the antioxidative capacity, obviously decreased in UC patients. Restoration of gut microbiota symbiosis provides an alternative strategy to prevent UC, which has been verified by the therapeutic feasibility of fecal microbiota therapy (FMT) strategy[19−21].

Recently, a 12-week phase II clinical trial revealed meaningful improvements on several efficacy indicators in active UC patients treated with apremilast (clinicaltrials.gov, NCT02289417). Compared with the placebo group (3.4%), the serious side effects occurred with a lower incidence in the 30 mg (0%) and 40 mg (1.8%) group, which indicated apremilast functioned as a safe and well-tolerant drug for UC patients[22]. Besides, the long-term efficacy and safety profile for an overall duration of 2 years are ongoing[22]. In the previous study, we have demonstrated that inhibition of PDE4 by apremilast exhibited the dose-dependent therapeutic effects on attenuating murine experimental acute mucosal inflammation, as evidenced by inhibiting the recruitment of inflammatory cells, maintaining the epithelial integrity, and suppressing the inflammatory responses in macrophages[23]. However, the pathological role of PDE4 in regulating the communication between epithelial barrier and immune system in the microecological environment of chronic UC remains ill-defined. Hence, in line with our previous work, dextran sulfate sodium (DSS)-induced murine chronic UC model was applied to reveal the effects and potential mechanism of inhibition of PDE4 by apremilast.

2. Methods and materials

2.1. Human studies

Colonic samples from patients with UC ($n = 5$) and healthy controls ($n = 4$) attending for clinically indicated endoscopy procedures were collected (Supporting Information Table S1). The biopsy samples were analyzed after obtaining informed written consent according to the approval of the Ethics Committee of the Ruijin Hospital Affiliated to Shanghai Jiao Tong University School of Medicine (Shanghai, China). Endoscopic biopsies were obtained from two sites: the active inflammatory site and fibrosis site.

2.2. Animals

All animal studies in this article are reported in compliance with the animal research: reporting of *in vivo* experiments (ARRIVE) guidelines. All experiments were conducted according to the National Institutes of Health Guide for Care and Use of Laboratory Animals, with the approval of the Bioethics Committee of Shanghai Institute of Materia Medica (SIMM), Chinese Academy of Sciences (CAS) (Shanghai, China). Male wide-type C57BL/6 mice (6−8 weeks old, 22−24 g, IACUC: 2018-11-TW-15),

obtained from Shanghai Laboratory Animal Center of Chinese Academy of Sciences (Shanghai, China), were used for the present studies. Animals were maintained with a 12-h/12-h light/dark cycle, 24 ± 2 °C and 55% ± 5% relative humidity.

2.3. Establishment and treatment of chronic ulcerative colitis

Experimental chronic UC was induced in the light of previous reports by Wirtz et al.[24]. Briefly, mice were obtained with three cycles of 2% DSS (36−50 kDa, MP Biomedicals, Irvine, CA, USA) in the drinking water for five days, which were closely followed by normal drinking water for successive 14 days. All mice, treated with DSS, developed severe colitis, and then were randomly divided into two experimental groups (DSS and DSS plus apremilast administration at the dose of 25 mg/kg) with 10 mice per group. Apremilast (Selleck, Houston, TX, USA) was orally administrated by gavage once daily at on Days 13−43, lasting for 30 days. Apremilast was dispersed in 0.5% carboxymethylcellulose sodium/0.25% Tween 80 (Sigma−Aldrich, St. Louis, MO, USA). In the end of experiment, blood samples were collected and centrifuged for determination of inflammatory cytokines.

For co-housing experiments, all mice were randomly divided into four groups, namely normal (housed separately, $n = 8$), vehicle (housed separately, $n = 8$), apremilast-treated group (housed separately, $n = 8$), and co-housing groups [8 mice received the solvent and 8 mice received apremilast (25 mg/kg)].

2.4. Bioluminescent imaging and intestinal permeability assay

In vivo living imaging with fluorescent fluorescein isothiocyanate (FITC)-dextran (Sigma−Aldrich) and chemiluminescent reagent L-012 sodium (Novus, Littleton, CO, USA) using IVIS Spectrum CT system were performed as previous reports[23,24].

2.5. Morphological and histological examination

During induction of chronic UC, disease activity index (DAI), including body weight loss, stool consistency, and occult blood, were monitored blind by 3 independent investigators according to the well-defined criterion[24,25]. By the end of experiment, murine colon tissues were removed for the following analysis. After recording the length of colons, the proximal colonic biopsy tissues were fixed in 10% formalin, buffered with phosphate buffered saline (PBS), and 5 μm slices were cut and incubated with hematoxylin and eosin (H&E). The severity of colonic inflammation and tissue damage were scored by 3 investigators from the Center for Drug Safety Evaluation and Research, SIMM, CAS (Shanghai, China).

2.6. Full-thickness colonic explants culture

Tissue parts (1 cm) were cut at the similar positions of colons and then cultured for 24 h in 1 mL of RPMI-1640 media (Gibco, Grand Island, NY, USA) in the presence of 10% fetal bovine serum (FBS, Hyclone, South Logan, UT, USA) in a humidified incubator of 5% CO_2 at 37 °C. The supernatants were centrifuged and stored for inflammatory mediators measurement.

2.7. Compositional analysis of the gut microbiota and data analysis

Next-generation sequencing library preparations and Illumina HiSeq 2500 sequencing were conducted at Shanghai Sangon Biotech Co., Ltd. (Shanghai, China). Fecal DNA extractions were performed as previously described[26]. Quality-tested libraries were sequenced using Illumina HiSeq 2500 and the extracted DNA from each sample was used to perform 16S rRNA analysis using PCR primers toward the V3−V4 regions. PCR products were detected on 1% agarose gels and then sequenced by MiSeq sequencer (Illumina, San Diego, CA, USA). Taxonomic analysis, heat map of species abundance cluster, principal coordinates analysis (PCoA), unweighted pair-group method with arithmetic mean (UPGMA), non-metric multidimensional scaling (NMDS), and analysis of similarities were performed.

2.8. Transmission electron microscopy

For ultrastructural analysis, mouse colonic tissues were excised and fixed in 2% paraformaldehyde and 2% glutaraldehyde (Sigma−Aldrich) in PBS according to previous description[27]. Tissue sections were monitored under a transmission electron microscopy (Philips Tecnai 20 U-Twin, Holland).

2.9. Preparation of single cell suspensions and flow cytometry analysis

Mesenteric lymph nodes (MLNs) and Peyer's patches (PP) were isolated sterilely and mononuclear cell suspensions were prepared as described[23,28]. Isolation of colonic LP was performed by successive digestions. Briefly, luminal contents and extraintestinal fat tissues of colonic biopsies were wiped off and subsequently colonic tissues were cut into small parts. Then, the tissues were first treated with HBSS (without Ca^{2+} and Mg^{2+}, Gibco) including 10% FBS and 5 mmol/L EDTA at 37 °C and shaken 15 min for three times to remove the mucus and epithelial cells, and subsequently, the pieces were digested by 0.5 mg/mL type IV collagenase (Sigma−Aldrich), 3 mg/mL dispase II (Sigma−Aldrich), and 0.1 mg/mL DNase I (Roche) in the RPMI-1640 media containing 10% FBS for 30 min. Digested cell suspensions were filtered with 70-μm cell strainers and applied to the following staining. Single cell suspensions were stained as previous reports[23]. Flow cytometry analyses were performed on BD LSRFortessa (BD Biosciences, San Jose, CA, USA) and all data were analyzed on FlowJo software (Tree Star, Ashland, OR, USA).

2.10. $CD4^+$ T cells purification and ex vivo stimulation

The $CD4^+$ T cells were purified from MLNs by using EasySep™ Mouse $CD4^+$ T Cell Isolation Kit (Stemcell, Vancouver, BC, Canada) according to the directions and *ex vivo* stimulated as previous description[23].

2.11. Cell cultures and treatment

HT-29 cells (Cat. HTB-38), human colon cancer cell line, U937 cells (Cat. CRL-1593), human myeloid leukemia cell line, THP-1 cells (Cat. TIB-202), human monocytic cell line, and Jurkat T cells (Cat. CRL-8129), human immortalized T cell line, were purchased from American Type Culture Collection (ATCC, Manassas, VA, USA). HT-29 cells were cultured in McCoy's 5a Medium (Gibco), and U937, THP-1, and Jurkat T cells were maintained in RPMI-1640 media including 10% FBS, 100 U/mL penicillin, and 100 μg/mL streptomycin in a humidified and homothermic incubator of 5% CO_2 at 37 °C. HT-29 cells were incubated with apremilast at the indicated concentrations with or without 100 ng/mL of TNF-α for 24 h

incubation for Western blot assay and for 3 h for real-time PCR (RT-PCR) assay. Additionally, siRNA transfected-HT-29 cells were treated with apremilast (10 μmol/L) and/or forskolin (adenylate cyclase activator, 10 μmol/L, Sigma−Aldrich) for additional 30 min to measure the phosphorylation of cAMP-response element binding protein (CREB).

2.12. SiRNA transfection in human epithelial cells

To knock down the catalytic subunit of PKA, human HT-29 cells were transfected with siRNA targeting PKA C-α (Cell Signaling Technology, Danvers, MA, USA), which was mixed in the Lipofectamine® RNAiMAX Reagent (Thermo Fisher Scientific, Waltham, MA, USA). HT-29 cells were collected and measured for PKA C-α expression after 48 h incubation.

2.13. Leukocyte's chemotaxis

Human HT-29 cells were treated with apremilast at the indicated concentrations in the presence of recombinant TNF-α (100 ng/mL). Human U937, THP-1, and Jurkat T cells were added into the upper chambers of Trans-well plates (Corning, NY, USA) in which the supernatants from TNF-α-primed HT-29 cells were plated into the lower chambers. After 2 h for chemotaxis, cells were amounted using hemocytometers.

2.14. Immunostaining analysis and immunohistochemistry

For colonic fibrosis, paraffin-embedded colon sections were stained with the picrosirius red reagents and the positive area of collagen deposition was observed under Olympus IX73 microscope (Tokyo, Japan). Mucus visualization was performed with Alcian blue staining. Briefly, the colonic sections were dewaxed, and then stained with Alcian blue/Nuclear Fast Red. For immunostaining of goblet cells, tissue sections were subjected to Periodic Acid-Schiff (PAS)/hematoxylin and the populations of PAS^+ goblet cells were observed under a light microscope (Olympus IX73). For immunohistochemistry, colonic slices were blocked with 3% H_2O_2 and soaked in citrate buffer solution for heat-induced epitope retrieval. Then, the sections were stained at 4 °C overnight with anti-α-smooth muscle actin (α-SMA) antibodies (Cell Signaling Technology, Cat. 19245) or anti-phosphodiesterase 4D (PDE4D) antibodies (Proteintech, Cat. 12918-1-AP, Wuhan, China), followed by incubation with streptavidin-horseradish peroxidase for 1 h. Then, the positive areas of colonic sections were developed using a diaminobenzidine substrate and the representative pictures were monitored under the Olympus IX73 microscope. For immunofluorescent determination, the sections were stained with anti-E-cadherin antibodies (Cell Signaling Technology, Cat. 3199), anti-occludin antibodies (Abcam, Cat. ab216327, Cambridge, MA, USA), anti-zonula occludens-1 (ZO-1) antibodies (Proteintech, Cat. 21773-1-AP), anti-CD11b antibodies (Abcam, Cat. ab18273), anti-Ly6G antibodies (BioLegend, Cat. 127609, San Diego, CA, USA), anti-CD3 antibodies (Abcam, Cat. ab5690), anti-intercellular adhesion molecule 1 (ICAM-1) antibodies (Abcam, Cat. ab179707), and anti-C-C chemokine receptor type 5 (CCR5) antibodies (Abcam, Cat. ab11466) overnight. The fluorescent signals were visualized by further conjugation with FITC or Alexa Fluor 647 anti-rabbit secondary antibodies and then counterstained with DAPI to visualize the nuclei (Abcam). The representative pictures were monitored under the Leica TCS SPS microscope (Wetzlar, Germany).

2.15. Inflammatory mediators determination

Colonic tissues were weighed and homogenized in PBS solution, then centrifuged at 16,260 $\times g$ for 10 min and the supernatants were stored for the assays. Cytokines in murine tissue homogenates and colon explants supernatants were quantified by mouse IFN-γ, TNF-α, IL-6, IL-12p40, and IL-17A enzyme-linked immunosorbent assay (ELISA) kits (BD Pharmingen, San Diego, CA, USA), mouse IL-1β, and IL-23 ELISA kits (Thermo Fisher Scientific). The supernatants from human HT-29 cells were assayed by human IL-8 and CXCL10 kits (BioLegend). Cytokines level in serum and colonic homogenates from UC patients were quantified by Luminex assay on the Luminex 200 instrument (Merck Millipore, Billerica, MA, USA) according to the manufacturer's directions.

2.16. RT-PCR analysis

Total RNA, extracted from colonic tissues by RNAsimple Total RNA Kit (Tiangen, Beijing, China), were reverse transcribed into cDNA using Hifair™ cDNA Synthesis Kit (Yeasen, Shanghai). Real-time quantitative PCR analysis was performed by SYBR® Green Realtime PCR Master Mix (Yeasen) plus 7500 Fast Real-Time PCR System (Applied Biosystems, Foster city, CA, USA) with gene-specific primers (Supporting Information Table S2). The expression level of genes was normalized to the internal housekeeping genes [glyceraldehyde-3-phosphate dehydrogenase (*GAPDH*) for human samples or β-actin for mouse samples].

2.17. Western blot assay

Colonic tissues and HT-29 cells were lysed with SDS lysis buffer, centrifuged, and then homogenized by Pierce BCA protein assay kit (Thermo Fisher Scientific). The protein samples were boiled for 10 min, electrophoresed in 10% SDS-PAGE, and then transferred to nitrocellulose membranes (Bio-Rad, Hercules, CA, USA). The blots were blocked with SuperBlock™ T20 blocking buffer (Thermo Fisher Scientific) and incubated at 4 °C with the appropriately diluted primary antibodies overnight. The signals were developed using the under ChemiDoc™ MP Imaging System (Bio-Rad).

2.18. Statistical analysis

Data are shown as mean ± standard error of the mean (SEM). Pearson correlation was performed using GraphPad Prism (Version 8.0, La Jolla, CA, USA). Statistical significance was determined by Student's *t*-test between two groups or one-way ANOVA with Dunnet's multiple comparisons test among three or more groups by GraphPad Prism 8.0 with no significant variance inhomogeneity in groups of more than two. $P < 0.05$ was considered statistically significant.

3. Results

3.1. Identification of the pathological role of PDE4 in chronic and relapsing UC patients

To reveal the pathological role of PDE4 in the colonic lesions of chronic and relapsing UC, the colonic biopsies from Chinese UC patients (Table S1) were collected and subjected to the following investigations. In line with the histopathological examinations that

mounting areas of mucosal ulcerations, loss of crypts and deposition of collagens were observed in the UC patients (Fig. 1A), we firstly identified the abnormal expression of PDE4 and dysfunction of signaling transduction in the colonic biopsies from UC patients (Fig. 1B and C). As illustrated in Fig. 1B−D, by contrast to the heathy individuals, PDE4A, PDE4B, PDE4C, and PDE4D were highly expressed in both the inflammation and inflammation-related fibrosis sites of UC patients, and consequently, the phosphorylation of CREB was decreased along with the pathological changes of PDE4. Moreover, Pearson correlation demonstrated that the expression levels of PDE4A, PDE4C, and PDE4D were positively correlated with the Mayo score of UC (Fig. 1D). Inspired by the findings, we further confirmed that destruction of epithelial barrier (Fig. 1B and C), mucosal inflammation, and recruitment of inflammatory cells emerged in the chronic UC patients (Fig. 1E and F). Taken together, our data represent the first study to reveal the pathological role of PDE4 in the gut microenvironment of UC patients.

3.2. *Inhibition of PDE4 attenuated the experimental manifestations of chronic UC*

Taken the pathological changes of PDE4 into consideration in chronic UC, inhibition of PDE4 by apremilast was conducted to uncover the therapeutic outcomes in DSS-induced chronic intestinal tissue damages. Compared to the vehicle controls (DSS only), oral administration of apremilast remarkedly attenuated the pathological features and disease severity of murine chronic UC, including body weight loss, gross bleeding, diarrhea, and colon shortening (Fig. 2A−C). Histopathological examination demonstrated that the vehicle mice exhibited obvious mucosal ulcerations, loss of epithelium and crypt's structure, as well as inflammatory cell infiltrations (Fig. 2D), which were consistent with the manifestations in UC patients (Fig. 1A). Whereas, apremilast-treated mice showed lesser tissue damages and lower histological scores than the vehicle mice (Fig. 2D). Additionally, colonic fibrosis and incapacitation are considered as the critical performances in the exacerbation of UC[29]. Picrosirius red staining and immunostaining with α-SMA indicated that apremilast could decrease the collagen depositions and activation of mucosal fibroblasts (Fig. 2E). Taken together, our findings implicated that inhibition of PDE4 by apremilast could ameliorate the chronic intestinal inflammation in experimental murine UC, which was further confirmed by *in vivo* imaging using the bioluminescent probe (Fig. 2F).

3.3. *Abnormal expression of PDE4 was observed and inhibition of PDE4 modulated cAMP-predominant PKA−CREB signaling in chronic UC*

Previous research has identified that apremilast is a highly specific PDE4 inhibitor with excellent suppressive effect on PDE4 enzymatic activity and displays effect to downregulate the expression of PDE4 isoforms in several inflammatory diseases[3,30]. To gain evidence toward the pathologic changes of PDE4 expression in the development of murine chronic UC models and whether apremilast exhibited suppressive effects on PDE4 isoforms expression, the mRNA and protein expression of PDE4 were investigated in this study. As illustrated in Fig. 2G, by contrast to normal mice, higher expression of *Pde4a*, *Pde4b*, and *Pde4d* were identified in DSS-treated mice. Consistently, the level of colonic cAMP (Fig. 2H) and phosphorylation of CREB were decreased (Fig. 2I), which could largely mimic the clinical features of UC patients (Fig. 1B−D). Inhibition of PDE4 by apremilast was able to decrease both the mRNA and protein level of PDE4 and subsequently promote the accumulation of cAMP and phosphorylation of CREB in the inflamed colonic tissues (Fig. 2G−J). Moreover, apremilast treatment could rectify the expression of cAMP-mediators, Epac1 and Epac2 (Fig. 2I). In accordance to our previous research, inhibition of PDE4 by apremilast could further directly lead to phosphorylation of CREB in human intestinal epithelial cells, HT-29 cells, without impacts on total CREB and PKA (Fig. 2K), which could be promoted by activation of adenylyl cyclase with forskolin (Fig. 2K). Whereas, phosphorylation of CREB could be blocked largely when the catalytic subunit of PKA was knocked down by siRNA transfection (Fig. 2K). Collectively, inhibition of PDE4 by apremilast displayed the impressive therapeutic effects through cAMP-dominant PKA−CREB signaling in chronic UC.

3.4. *Inhibition of PDE4 maintained the intestinal mucosal physical barrier function in chronic UC*

As the vital physical and chemical defense against heterologous antigens, the intestinal barrier is extremely indispensable to maintain the mucosal homeostasis[31]. To clarify the effects of inhibition of PDE4 on mucosal barrier function in chronic UC, we conducted *in vivo* fluorescent imaging and intestinal permeability assay through FITC-dextran administration. The results demonstrated that inhibition of PDE4 by apremilast obviously reduced the accumulation of positive signals in the abdominal mucosa (Fig. 3A) and the serum fluorescence degree of FITC (Fig. 3B) in chronic UC. Transmission electron microscopy (TEM) observations showed that by contrast to normal controls, the intestinal epithelial cells were disordered with vesicular or vacuolated mitochondria and other organelles and enlarged cell junctions in vehicle mice (Fig. 3C). Consistently, apremilast exhibited capacity to improve the ultrastructural abnormalities of the epithelial cells (Fig. 3C). Further *in situ* visualization, protein and mRNA expression assay of tight junction proteins confirmed that apremilast protected the architecture and integrity of epithelium in the inflamed colonic tissues (Fig. 3D−F). Moreover, abnormal expression of claudins, including decreased claudin-1 and increased claudin-2, and increased expression of matrix metalloproteinases (MMPs) were also redressed following apremilast treatment (Fig. 3E−G), which were in line with the evidence that apremilast dose-dependently reduce the level of *MMP3* from TNF-α-driven human HT-29 cells (Fig. 3H).

3.5. *Inhibition of PDE4 rebuilt the mucosal immune homoeostasis in chronic UC*

Disturbed physical barrier function pathologically results in exposure of PAMPs and DAMPs and burst of mucosal inflammation[32]. We then rationalized that inhibition of PDE4 exerted improvement on mucosal homeostasis. As observed in colonic LP, myeloid cells, neutrophils, macrophages, DCs, and monocytes were obviously increased in chronic UC, and apremilast treatment could reverse these changes (Fig. 4A), which were confirmed by immunofluorescent visualization with CD11b and Ly6G (Fig. 4B). Consistently, decreases of the population of myeloid cells, neutrophils, macrophages, and DCs upon apremilast treatment were also seen in the surrounding lymphoid organs of intestine, including mesenteric lymph nodes (MLNs) and PP (Supporting

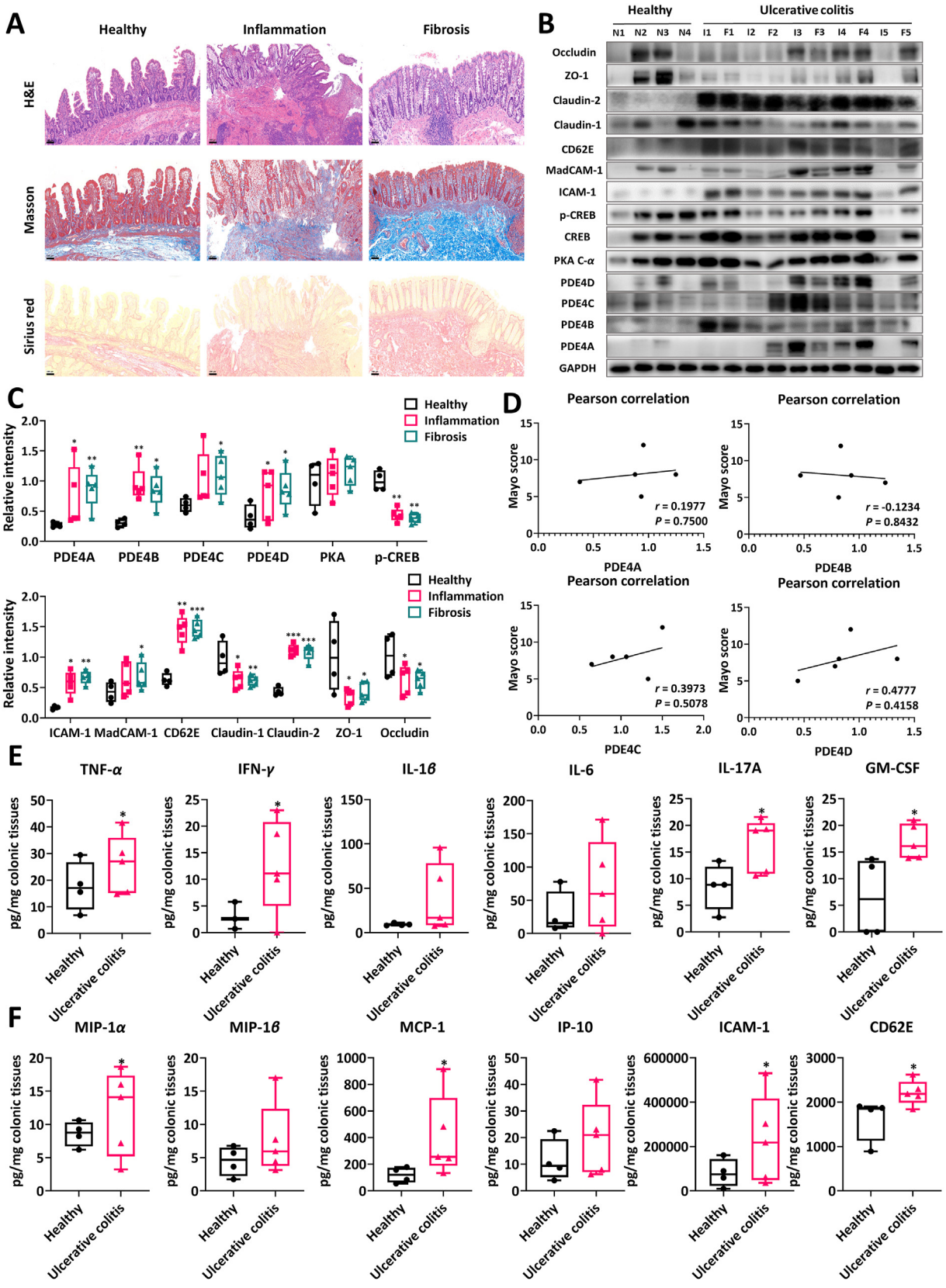

Figure 1 Abnormal expression of PDE4 and signaling transduction were observed in chronic UC patients. (A) Representative images of H&E, Masson, and Sirius red staining of the colonic biopsies of UC patients. Scale bar: 100 μm. (B) Western blot analyses of protein expression of the colonic biopsies. (C) Quantification analyses of Western blot results. (D) Pearson correlation of PDE4 expression and Mayo score of UC. *P* values represented the significance level and *r* values represented the coefficient of association. (E) The inflammatory cytokines in colonic homogenates of UC patients were examined by Luminex assay. (F) The chemokines and adhesive molecules in colonic homogenates of UC patients were examined by Luminex assay. Data are presented as mean ± SEM; $n = 4$ for healthy controls, $n = 5$ for UC patients. *$P < 0.05$, **$P < 0.01$, ***$P < 0.001$ *vs.* healthy controls.

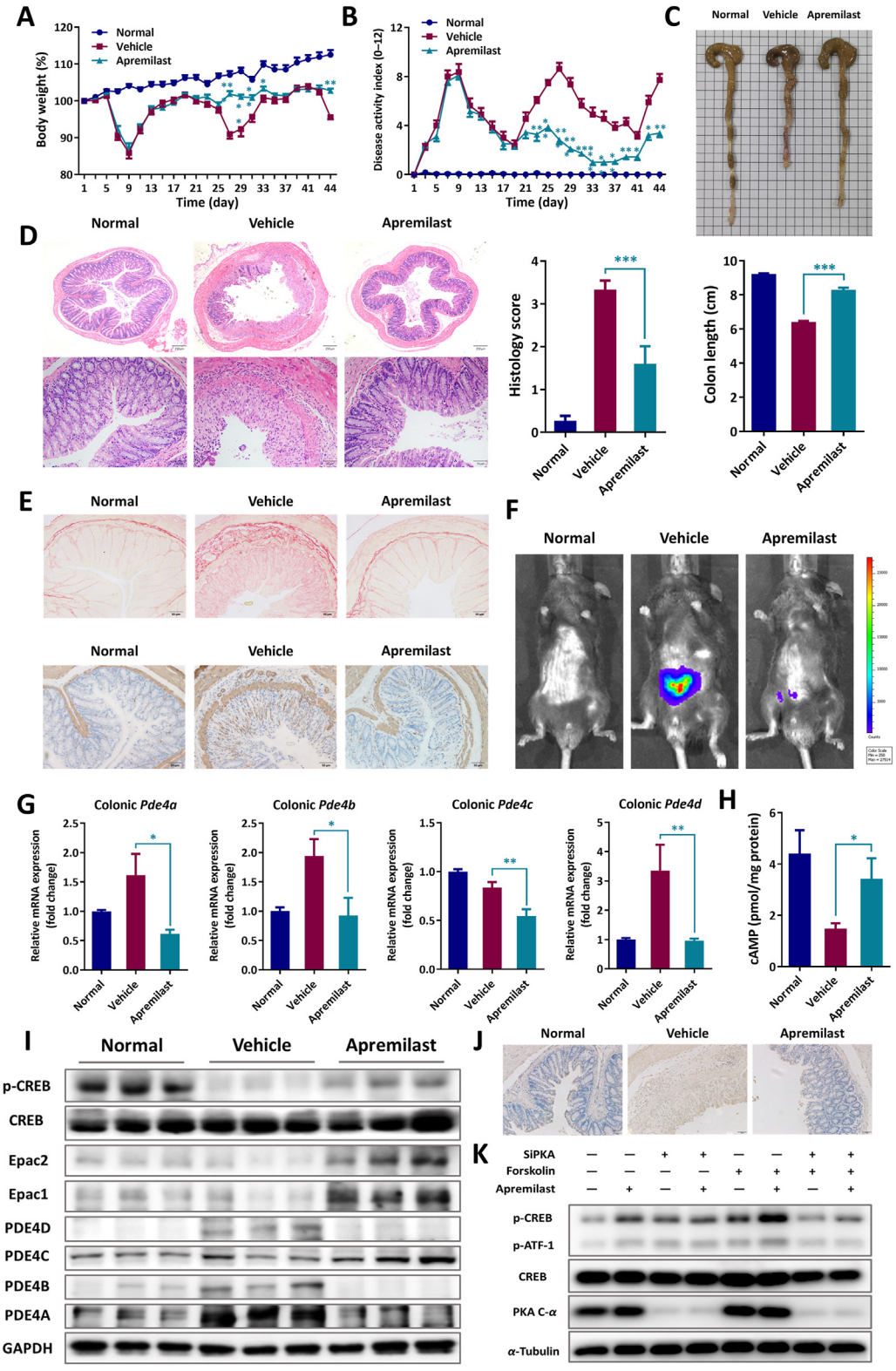

Figure 2 Apremilast attenuated the clinical manifestations and mucosal inflammation in chronic UC. (A) Body weight change, indicated as the percentage of initial weight. (B) Disease activity index (DAI). (C) Representative colon pictures and colonic length. (D) Representative H&E staining (40× and 200× magnification), and histopathological scores. Scale bar: 250 μm (upper), and 75 μm (bottom). (E) Representative staining of picrosirius red (upper, 200× magnification) and α-SMA (bottom, 200× magnification). Scale bar: 50 μm. (F) Representative pictures of bioluminescent imaging with L-012. (G) The mRNA expression of the isoforms of PDE4. (H) The cAMP levels in the inflamed colonic tissues. (I) Western blot analyses of PDE4 and its related proteins. (J) Representative staining of PDE4D in colonic sections. Scale bar: 50 μm. (K) Western blot assay of phosphorylation of CREB in apremilast and/or forskolin treated siPKA transfected-HT29 cells. Data are presented as mean ± SEM; $n = 10$ mice per group. $^{*}P < 0.05$, $^{**}P < 0.01$, $^{***}P < 0.001$ *vs.* vehicle group.

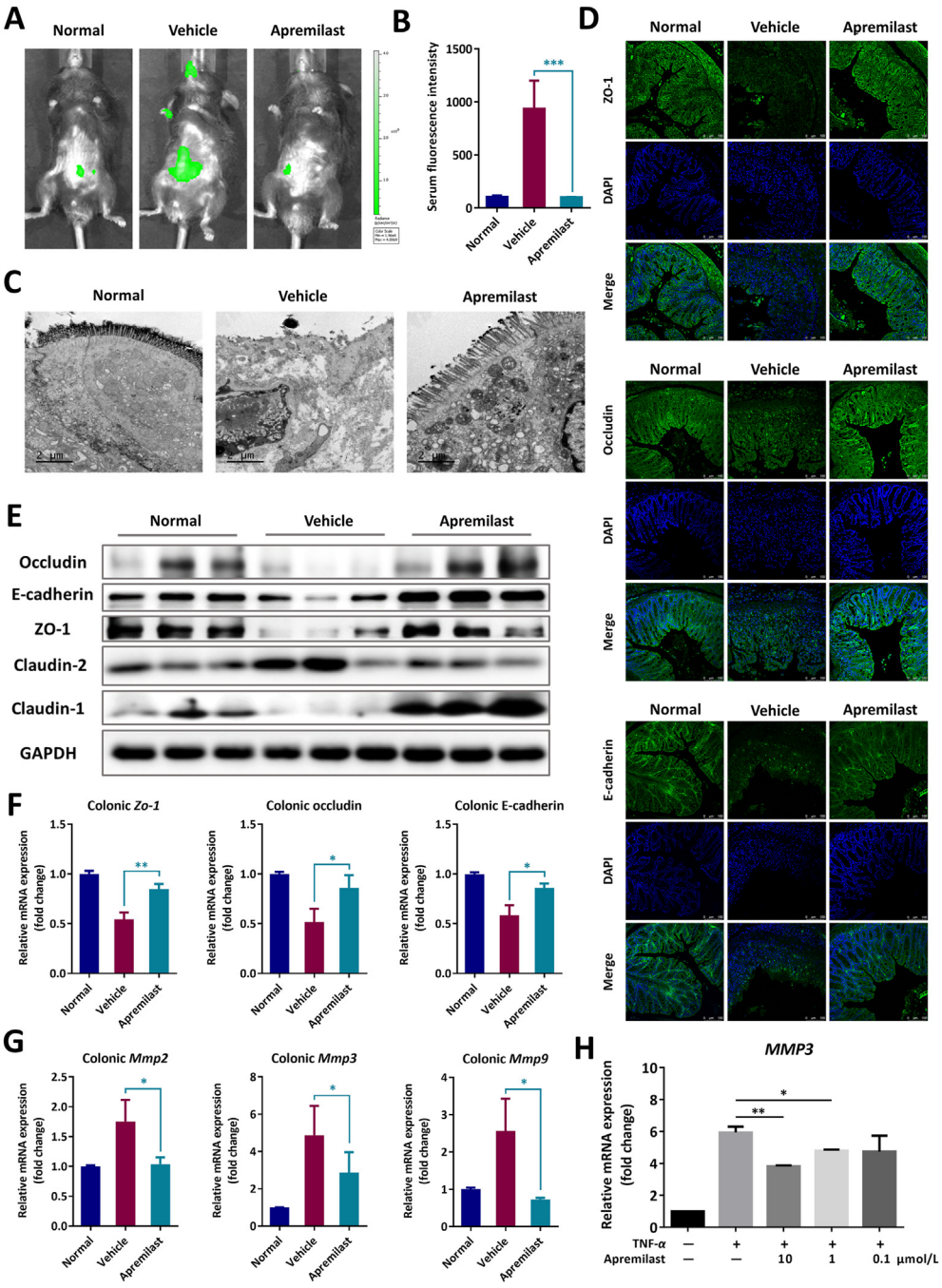

Figure 3 Apremilast maintained the intestinal barrier function and protected the epithelial integrity in chronic UC. (A) Representative pictures of fluorescent imaging with FITC-dextran. (B) Serum fluorescence intensity of FITC-dextran. (C) Representative images of colonic ultrastructure under a transmission electron microscope (6400× magnification). Scale bar: 2 μm. (D) Representative immunofluorescent staining with ZO-1, E-cadherin, and occludin (200× magnification). Scale bar: 100 μm. (E) Western blot assay of tight junction proteins. (F) The mRNA expression of tight junction proteins in inflamed colonic tissues. (G) The mRNA expression of matrix metalloproteinases in inflamed colonic tissues. (H) The mRNA expression of *MMP3* in TNF-α-stimulated HT-29 cells. (A)−(G) Data are presented as mean ± SEM; $n = 10$ mice per group. (H) Data are presented of three independent experiments. $^{*}P < 0.05$, $^{**}P < 0.01$, $^{***}P < 0.001$.

Information Fig. S1). Besides, apremilast could also interfere with the infiltration and activation of NK cells, referring to CD27 and CD335 expression on $CD3^{-}NK1.1^{+}$ cells from the inflamed LP, MLNs, and PP (Fig. 4C and Supporting Information Fig. S2). In addition to innate immunity, abnormal activation of adaptive immunity also plays an important role in the deterioration of chronic UC. In the present study, we found that apremilast could suppress the polarization of Th1 and Th17 cells in LP (Fig. 4D). In line with flow cytometry analysis, colonic sections staining with CD3 revealed that T cells were mostly scattered across the mucosal and submucosal layers and the total number of T cells in apremilast-treated mice was lower than that in vehicle mice (Fig. 4E). Meanwhile, apremilast treatment reduced the percentage of IFN-γ and IL-17-producing cells in MLNs and LP (Supporting

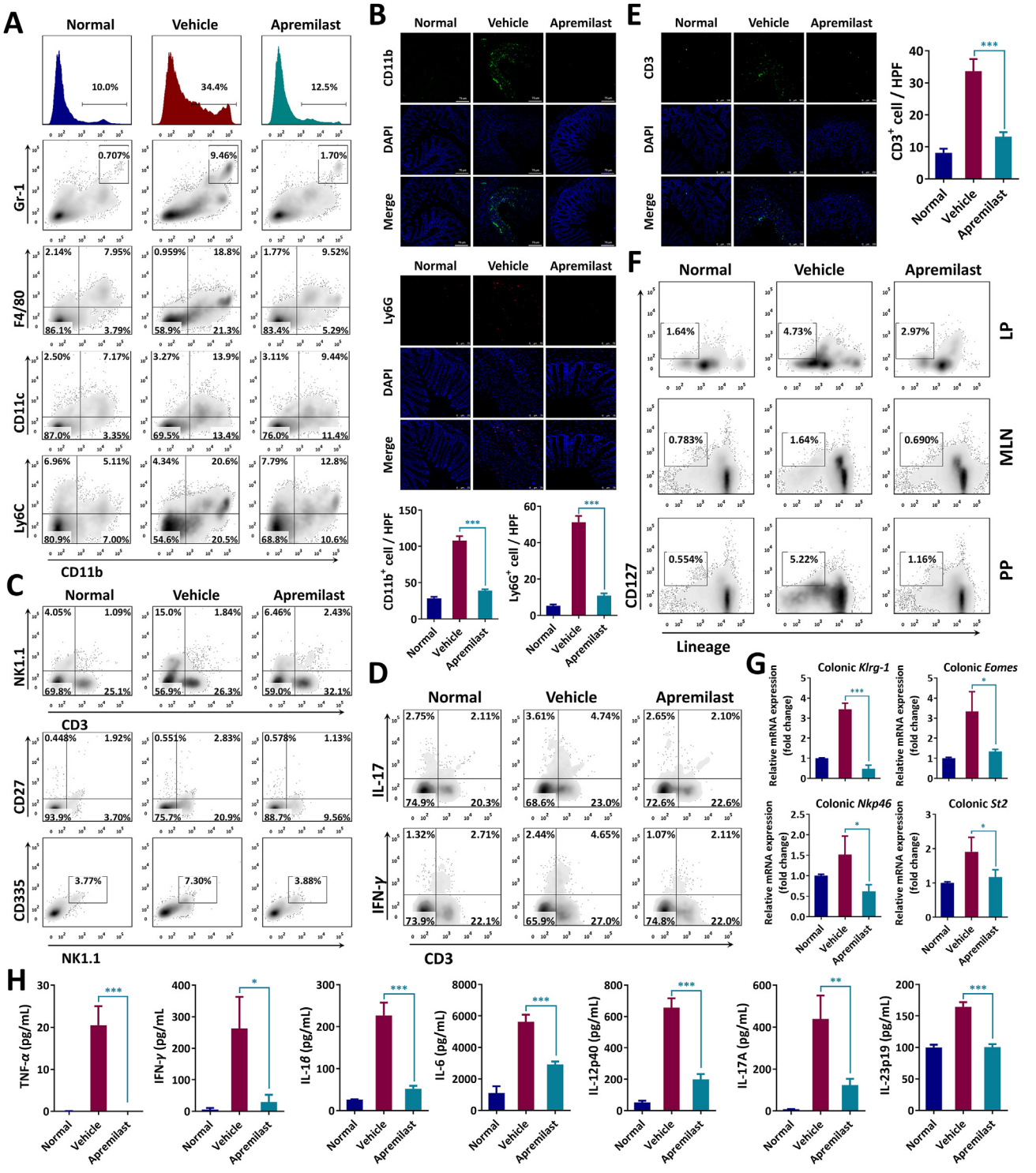

Figure 4 Apremilast maintained the mucosal immune homeostasis in chronic UC. (A) The percentage of myeloid cells ($CD11b^+$), neutrophils ($CD11b^+Gr\text{-}1^+$), macrophages ($CD11b^+F4/80^+$), dendritic cells ($CD11b^+CD11c^+$), and monocytes ($CD11b^+Ly6C^+$), in colonic lamina propria (LP). (B) Representative CD11b and Ly6G (200× magnification), and quantitative statistics. Scale bar: 75 μm. (C) The percentage of NK cells ($CD3^-NK1.1^+$) and flow cytometry analysis of activation of NK cells (CD27 and CD335 positive expression) in colonic LP. (D) The expression of IFN-γ and IL-17 in $CD3^+$ T cells in colonic LP, analyzed by flow cytometry. (E) The representative images of immunofluorescent staining with CD3 (200× magnification) and quantitative statistics. Scale bar: 100 μm. (F) Flow cytometry analysis of the population of innate lymphoid cells (ILCs) in Peyer's patches (PP), mesenteric lymph nodes (MLNs), and colonic LP. (G) The mRNA expression of transcriptional factor related to activation of NK cells and ILCs. (H) The level of inflammatory cytokines in the colonic explants. Data are presented as mean ± SEM; $n = 10$ mice per group. $^*P < 0.05$, $^{**}P < 0.01$, $^{***}P < 0.001$.

Information Fig. S3A and B). Moreover, compared to vehicle mice, the proliferation and cytokines release capacity of $CD4^+$ T cells, purified from MLNs, were largely impeded in mice-received apremilast (Supporting Information Fig. S3C and D).

Increasing evidence suggested that ILCs functioned as the important regulators in the pathological process of mucosal inflammation and barrier function, mainly due to the rapid initiation of cellular responses to internal or extra signals such as neuronal mediators, alarmins, and microbial environmental cues in the gut lumen[13,14,33]. Herein, we identified the well-considered population of ILCs, labelled as lineage$^-$CD127$^+$ on $CD45^+$ leukocytes, which were highly increased in the inflamed LP, MLNs, and LP and were reversed following apremilast treatment in chronic UC (Fig. 4F). Furthermore, apremilast decreased the specific transcriptional factors, including NK cell p46-related protein (*Nkp46*), killer-cell lectin like receptor G1 (*Klrg-1*), suppression of tumorigenicity 2 (*St2*), and eomesodermin (*Eomes*) (Fig. 4G). Given the accumulative effects of multiple immune cell infiltrations with in the gut microenvironment, we further measured the inflammatory cytokines, such as TNF-α, IFN-γ, IL-1β, IL-17A, and IL-23p19, in the colonic explants and colonic homogenates. As presented in Fig. 4H and Supporting Information Fig. S4, by contrast to vehicle mice, both the mRNA and protein level of several cytokines were reduced in apremilast-treated colitic mice.

3.6. Inhibition of PDE4 modulated the communication between epithelial and immune cells in chronic UC

To gain detailed molecular mechanism for immune cell recruitments, mRNA and protein levels of adhesive molecules, chemokines, along with the corresponding receptors were monitored (Fig. 5). Therapeutically, apremilast treatment could suppress the mRNA levels of several chemokines and chemokine receptors (Fig. 5A and C), which were affirmed by immunofluorescent staining with CCR5 (Fig. 5B). Moreover, we also found that apremilast could downregulate the expression of adhesive molecules, *Icam-1*, mucosal vascular addressin cell adhesion molecule 1 (*Madcam-1*), and *Cd62e* (Fig. 5D–F). *In vitro*, the communication between human epithelial cells, HT-29 cells, and immune cells, Jurkat T, U937, and THP-1 cells, was performed to directly verify our findings. As illustrated in Fig. 5G–I, TNF-α obviously led to Jurkat T, U937, and THP-1 cells migrating to the monoculture of HT-29 cells and apremilast displayed a dose-dependent manner to inhibit chemotaxis of immune cells, mainly attributing to suppressing the expression of ICAM-1, CD62E, IP-10, and IL-8 from TNF-α-primed human HT-29 cells.

3.7. Inhibition of PDE4 modulated the diversity and composition of gut microbiota in chronic UC

Mucosal homeostasis refers to the crosstalk and communications between the gut lumen and intestinal mucosa. To deeply understand the role of apremilast in the intestinal microecological environment, gut microbiota, a principal factor in the pathogenesis of UC, was assessed by 16S rRNA sequencing analysis in the fecal samples of chronic UC. In total, 885,121 useable reads and 265 operational taxonomic units (OTUs) were obtained from 9 samples by Illumina HiSeq 2500, which revealed that 242, 249, and 234 OTUs were presented in the normal, vehicle, and apremilast-treated mice (Fig. 6A). PERMANOVA analysis indicated there existed a difference among the composition of microbiota from three groups (Fig. 6B). Meanwhile, the system clustering tree based on unweighted pair-group method with arithmetic mean verified the results and further suggested that the distance from the normal group to the apremilast-treated group was smaller than that to vehicle group (Fig. 6C), which were also revealed in the heatmap of sample clustering (Fig. 6D). Moreover, PCoA (Fig. 6E) and NMDS (Fig. 6F) analysis showed a markedly distinct gut microbial landscape in the normal, vehicle, and apremilast-treated groups. We further investigated the gut microbiota species and their relative abundance. At the genus level, over 20 genera could be found in all samples and the most abundant genera in all samples were *Muribaculaceae*, *Akkermansia*, and *Lactobacillus* (Fig. 6G). Relative to vehicle mice, apremilast treatment decreased the genus levels of colitis-related microbes, but increased the levels of beneficial microorganisms, such as *Lactobacillus* and *Bifidobacterium* (Fig. 6G). The detailed composition and abundance in species level were illustrated as heat map of sample clustering in Fig. 6H. In summary, our results showed that apremilast treatment could modulate the gut microbiota composition in experimental chronic UC.

3.8. Inhibition of PDE4 restored the colonic chemical barrier function in chronic UC

Disturbance of gut microbiota is closely associated with dysfunction of mucins and antimicrobial peptides (AMPs), mainly derived from goblet cells, which contribute to the destruction of mucosal homeostasis in UC[34]. As presented in Fig. 7A and B, loss of goblet cells and mucus by PAS and Alcian blue staining were observed in colitic mice, and were attenuated upon apremilast therapy. Accordingly, quantitative PCR results showed apremilast could increase the expression of Mucin-2 (MUC2, Fig. 7C and D). Meanwhile, apremilast also modulated the mRNA expression of caudal type homeobox 2 (*Cdx2*), a positive indicator of MUC2 expression (Fig. 7E), and trefoil factor 3 (*Tff3*), a regulatory factor mediating the mucosal barrier function (Fig. 7F). Furthermore, we examined the production of AMPs and expression of S100 proteins and alarmins, which demonstrated that increased levels of *Cap18*, cathelicidin, and lysozyme (Fig. 7G), as well as S100A4, S100A8, S100A9, S100A10, and heat shock protein 90 (*Hsp90*), were aborted in apremilast-treated colitic mice (Fig. 7D, H, and I). Consistently, apremilast could suppress the expression of S100A9 from TNF-α-driven human HT-29 cells (Fig. 7J). Briefly, the findings indicated that inhibition of PDE4 by apremilast could maintain the intestinal physical and chemical barrier function in chronic UC.

3.9. Gut microbiota is partially responsible for the therapeutic effects of apremilast in chronic UC

To probe whether the rearranged gut microbiota was involved in the effects of apremilast on mucosal homeostasis, we conducted the transmissible nature of the gut microbiota by co-housing apremilast-treated mice with colitic mice. Interestingly, in the development of chronic UC, the body weight loss, diarrhea, stool bleeding, colon shortening, and splenomegaly in co-housed vehicle group were weaker than those in separately housed vehicle group (Fig. 8A–C); On the contrary, the disease severity in apremilast-treated group were worse than those in separately housed apremilast-treated group (Fig. 8A–C). We also observed significant increase of mucosal ulcerations and loss of epithelium in apremilast-treated mice, compared with separately housed mice, which suggested that the intestinal inflammation of chronic UC in co-housed mice tended to be an intermediate state

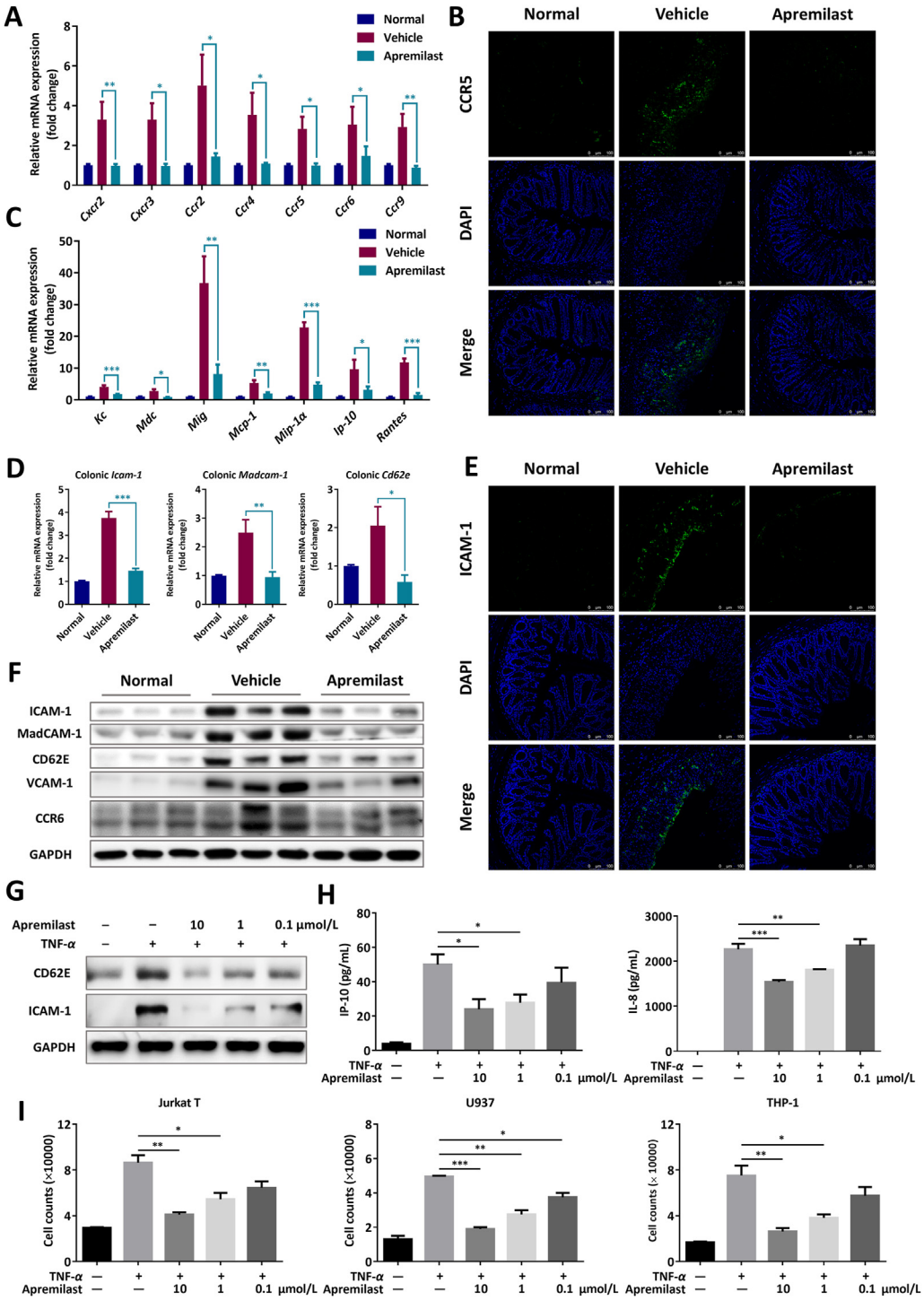

Figure 5 Apremilast suppressed the expression of several adhesive molecules, chemokines, and chemokine receptors in chronic UC. (A) The mRNA expression of multiple chemokine receptors in inflamed colonic tissues. (B) Representative immunofluorescent staining of CCR5 (200× magnification) in colon sections. Scale bar: 100 μm. (C) The mRNA expression of several chemokines in inflamed colonic tissues. (D) The mRNA expression of *Icam-1*, *Madcam-1*, and *Cd62e* in inflamed colonic tissues. (E) Representative immunofluorescent staining of ICAM-1 (200× magnification) in colon sections. Scale bar: 100 μm. (F) Western blot assay of adhesive molecules and chemokine receptors in inflamed colonic tissues. (G) Western blot assay of ICAM-1 and CD62E expression in HT-29 cells. (H) IP-10 and IL-8 levels in TNF-α-cultured HT-29 cells, detected by ELISA. (I) The counts of Jurkat T, U937, and THP-1 cells chemotactic to the lower chambers. (A)−(F) Data are presented as mean ± SEM; $n = 10$ mice per group. (G) Data are presented of three independent experiments. (H, I) Data are presented as mean ± SEM ($n = 3$). *$P < 0.05$, **$P < 0.01$, ***$P < 0.001$.

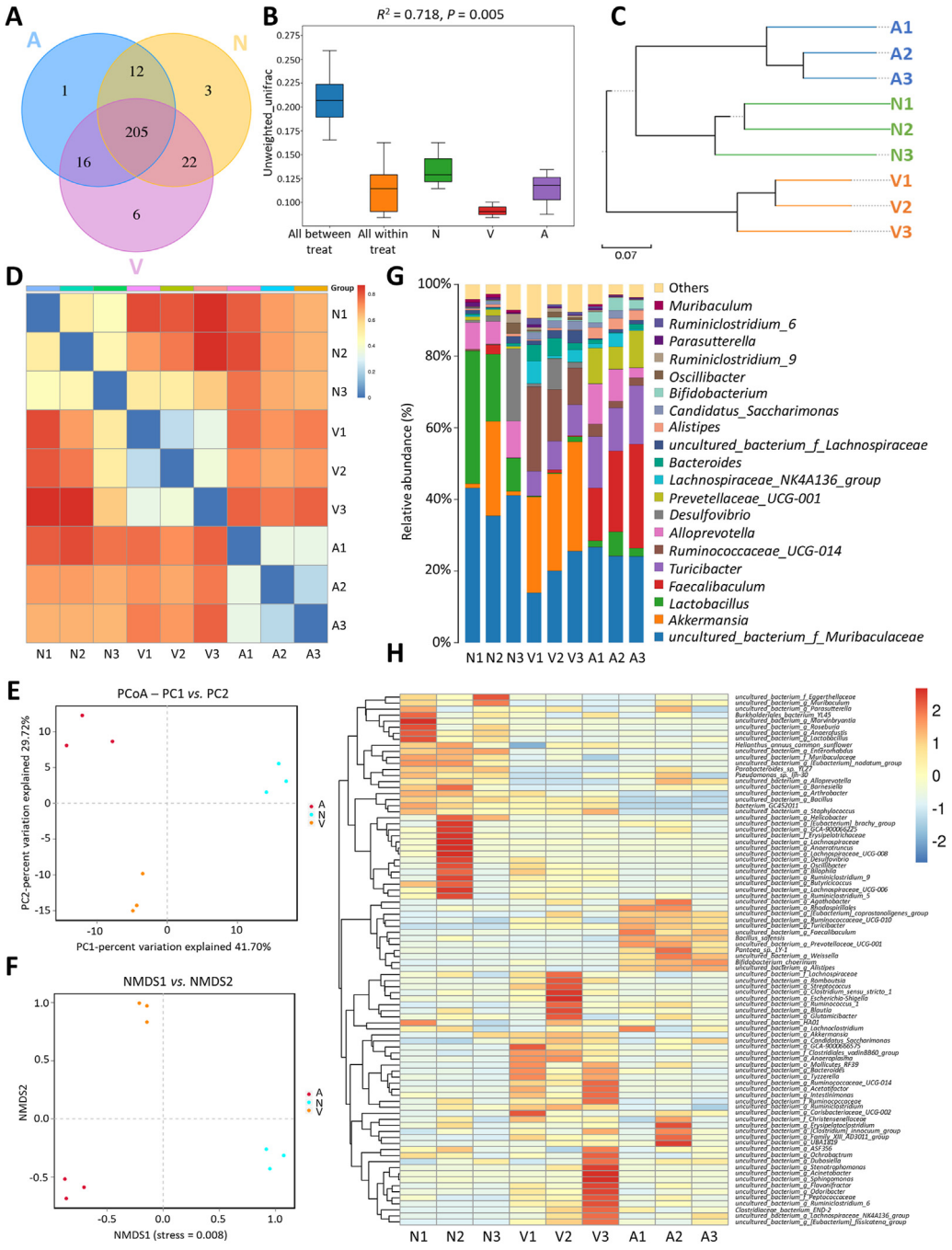

Figure 6 Apremilast remodeled the composition of gut microbiota in chronic UC. (A) The Venn diagram of OTUs in each group. (B) PERMANOVA/Anosim analysis. (C) Unweighted pair-group method with arithmetic mean (UPGMA). (D) Sample heat map analysis based on β-diversity. (E) Principal coordinates analysis (PCoA). (F) Non-metric multidimensional scaling (NMDS). (G) Composition of microbiota at genus level. (H) Heat map of cluster of species abundance.

(Fig. 8D). Further 16S rRNA analysis revealed an equilibrated gut microbial landscape in the co-housed mice (Fig. 8E and F) and demonstrated that the abundance of some inflammation-associated OTUs in apremilast-treated mice were increased after co-housing, while the inflammation-associated OTUs were decreased in co-housed vehicle mice (Fig. 8G–I).

Consistent with these findings, the modulatory effects of apremilast on mucosal homeostasis were compromised by co-housing, as evidenced by the proportions of inflammatory cells in LP and secretion of inflammatory cytokines in the colonic explants (Fig. 9). In keeping with the results in Fig. 4, by contrast to separately housed mice, the percentage of APCs, activated NK cells, Th1 cells, Th17 cells, and ILCs were obviously increased in co-housed apremilast-treated mice and decreased in co-housed vehicle mice (Fig. 9A–D). Additionally, the production levels of TNF-α, IFN-γ, IL-12p40, and IL-17A were highly increased in co-housed apremilast-treated mice, compared to separately housed mice (Fig. 9E), which collectively suggested that the transferred gut microbiota from vehicle mice to apremilast-treated mice by co-housing contributed to more severe symptoms and mucosal inflammation in chronic UC.

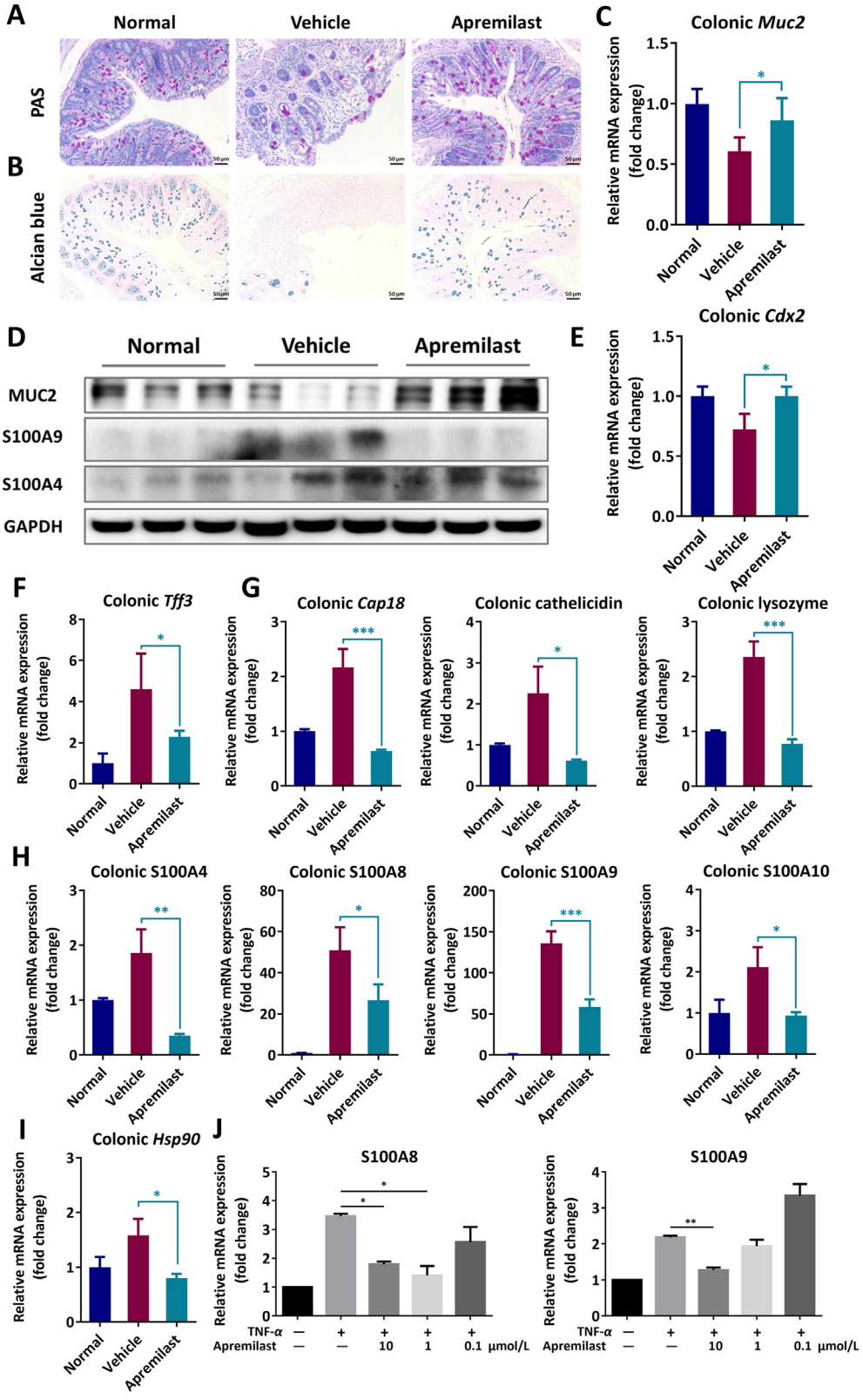

Figure 7 Apremilast rectified the colonic mucus homeostasis and the expression of antimicrobial peptides in chronic UC. (A) Representative PAS-stained goblet cell images (200× magnification). (B) Representative images of Alcian blue-stained mucus layer (200× magnification). Scale bar: 50 μm. (C) The mRNA expression of *Muc2* in colonic tissues. (D) Western blot assay of MUC2, S100A4, and S100A9 in colonic tissues. The mRNA expression of *Cdx2* (E), *Tff3* (F), antimicrobial peptides (G), S100 proteins (H), and *Hsp90* (I) in colonic tissues. (J) The mRNA expression of S100A8 and S100A9 in TNF-α-stimulated HT-29 cells. (A)−(I) Data are presented as mean ± SEM; $n = 10$ mice per group. (J) Data are presented as mean ± SEM ($n = 3$). $^{*}P < 0.05$, $^{**}P < 0.01$, $^{***}P < 0.001$.

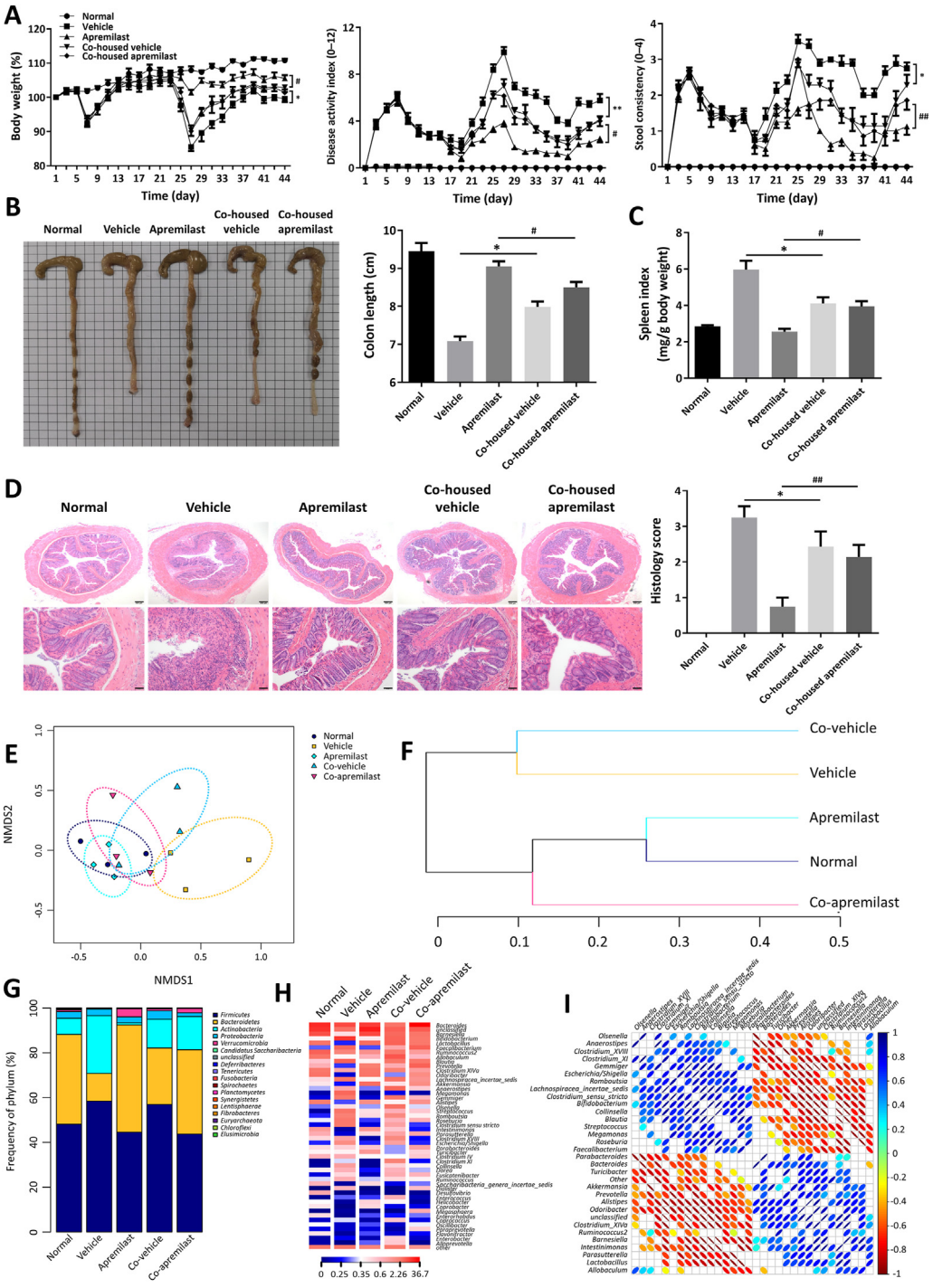

Figure 8 Gut microbiota is responsible for the therapeutic effects of apremilast in chronic UC. (A) Body weight change, DAI, and stool consistency scores. (B) Representative colon pictures and colonic length. (C) Spleen index, indicated as the weight of spleens (mg)/body weight (g). (D) Representative H&E staining (40× and 200× magnification) and histopathological scores. Scale bar: 250 μm (upper), and 50 μm (bottom). (E) NMDS analysis. (F) Unweighted pair-group method with arithmetic mean (UPGMA). (G) Composition of microbiota. (H) Heat map of cluster of microbiota abundance. (I) Correlation of OTUs. (A)−(D) Data are presented as mean ± SEM; $n = 8$ mice per group. (E)−(I) $n = 3$ mice per group. $^{*}P < 0.05$, $^{**}P < 0.01$; $^{\#}P < 0.05$, $^{\#\#}P < 0.01$.

4. Discussion

UC is one of the two major forms of inflammatory bowel diseases (IBD), which are closely linked with the precise interaction between gut microbiota, intestinal epithelial barrier function and mucosal immunity[15]. It has been demonstrated that targeting the cAMP-specific PDE4 displayed dramatic effects on suppression of cytokines in multiple inflammatory cells, including macrophages, NKT cells, neutrophils, and T helper cells, and intestinal epithelial cells[35–37]. In the past decades, though the PDE4 inhibitors, rolipram, tetomilast, and roflumilast have been investigated in experimental colitis, the adverse effects impeded the further

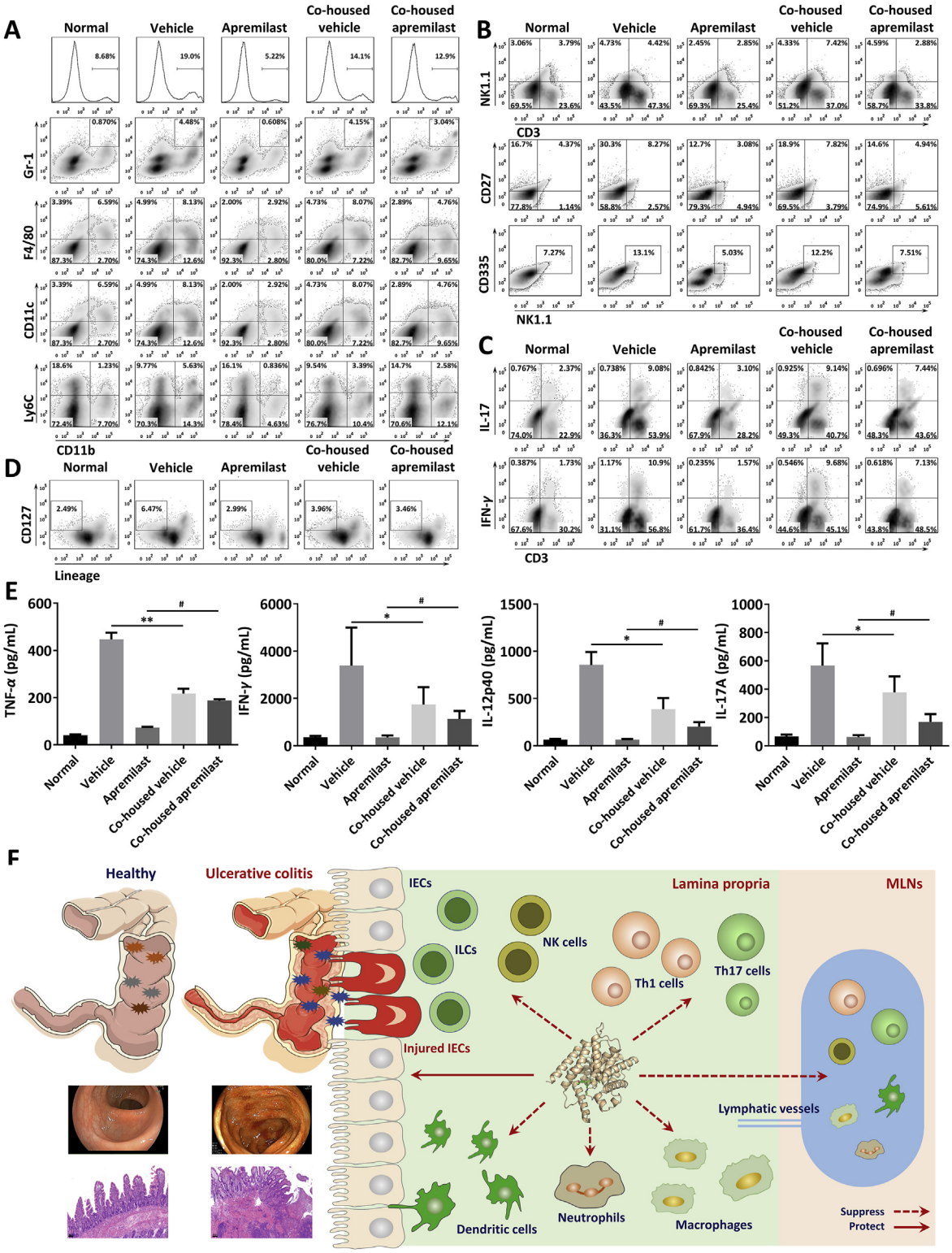

Figure 9 Effect of co-housing on apremilast in attenuating the inflammatory infiltrations and mucosal inflammation in chronic UC. (A) The percentage of myeloid cells ($CD11b^+$), neutrophils ($CD11b^+Gr\text{-}1^+$), macrophages ($CD11b^+F4/80^+$), dendritic cells ($CD11b^+CD11c^+$), and monocytes ($CD11b^+Ly6C^+$), in colonic LP, assayed by flow cytometry. (B) The percentage of NK cells ($CD3^-NK1.1^+$), and activation of NK cells (CD27 and CD335 positive expression), in colonic LP, assayed by flow cytometry. (C) The expression of IFN-γ and IL-17 in $CD3^+$ T cells in colonic LP, analyzed by flow cytometry. (D) Flow cytometry analysis of the population of ILCs in colonic LP. (E) The level of inflammatory cytokines in the colonic explants, assayed by ELISA. (F) The schematic diagram of targeting PDE4 in attenuating chronic UC through modulating mucosal homeostasis. Scale bar: 100 μm. Data are presented as mean ± SEM; $n = 8$ mice per group. $^*P < 0.05$, $^{**}P < 0.01$; $^{\#}P < 0.05$.

clinical application[1,35]. By contrast, apremilast is a well-tolerated PDE4 inhibitor with little gastrointestinal side effects[38]. In our previous report, we elucidated that apremilast exerted protective efficacies in murine acute UC, which is the first report to uncover its therapeutic capacity in DSS-induced acute mucosal inflammation[23]. However, the pathological function of PDE4 in regulating the communication between epithelial barrier and immune system in the microecological environment of chronic UC, a more complicated scenario than acute phase, remains undefined. Hence, the present research was aimed to reveal the therapeutic effects and the underlying mechanism of inhibition of PDE4 by apremilast, which indicated that apremilast could significantly alleviate the pathological features and modulating the mucosal homeostasis from the gut lumen to the mucosal immune system, including ameliorating the disturbance of gut microbiota, dysfunction of epithelial barrier, intestinal fibrosis, and overactivation of mucosal immune cells (Fig. 9F).

Recently, single-cell RNA sequencing (scRNA-seq) revealed that defective cAMP-response signaling pathway, referring to the multiple intracellular defects and PDE4B/TNF-α-expressing macrophages were found in pediatric-onset colitis and the phosphodiesterase inhibitor dipyridamole could improve the clinical symptoms in DSS-induced murine colitis and pediatric colitis patients[39]. Moreover, genome-wide association studies (GWAS) analysis identified a missense variant in ADCY7 that led to distraction of cAMP production in UC[17]. Consistently, we identified the decreased level of cAMP in the inflamed tissues of murine chronic UC (Fig. 2H). Moreover, gene expression of PDE4 isoforms in peripheral blood mononuclear cells (PBMCs) from adult patients with inflammatory diseases indicated that the mRNA expression of PDE4C was largely increased in patients with CD *versus* healthy individuals[3]. To gain evidence toward the pathology of PDE4 in chronic mucosal inflammation, investigations were performed. It's worth mentioning that overexpression levels of PDE4 and defective cAMP-dominant signaling pathway were firstly identified in chronic UC patients in the present study. Moreover, dysfunction of PDE4 and its related signaling pathway were observed in DSS-induced chronic UC, which provide the critical clue for the pathological role of PDE4 in initiating the mucosal inflammation and disturbance of gut homeostasis. Consistently, inhibition of PDE4 by apremilast could downregulate the mRNA and protein expression of PDE4 and then modulating the phosphorylation of CREB and the expression of cAMP-mediators (Fig. 2G−K).

The epithelium is comprised by the formation of tight junctions between the constitutive epithelial cells, which represents an essential part in modulating the mucosal homeostasis. Up to now, claudins, occludin, scaffold protein zonula occludens, and junctional adhesion molecules have been well-identified in maintaining the intestinal permeability[7]. In experimental chronic UC, we identified the disarranged intestinal barrier function and abnormal ultrastructure of epithelial cells (Fig. 3A−C). Apremilast treatment could maintain a normal intestinal physical barrier function by upregulating the expression of tight junction proteins (Fig. 3D and E). Integrins are expressed at the cell surfaces through binding to adhesion molecules and mediating inflammatory infiltrations[12]. Leukocytes migration from peripheral circulation into the inflamed colonic tissues are tightly modulated by the precise interaction between $\alpha4\beta7$ integrin and its ligands, MadCAM-1[40]. Proinflammatory cytokines, including IL-1 and TNF-α could upregulate the expression of ICAM-1, E-selectin, and MadCAM-1 and integrin-based therapeutic approaches have suggested positive outcomes in patients with IBD[41]. Accordingly, the expression of ICAM-1, MadCAM-1, and E-selectin were increased in chronic UC (Fig. 5D−F) and TNF-α-driven HT-29 cells (Fig. 5G).

The gut microenvironment is characterized by the sophisticated and complicated network between the epithelium and microbiome, which plays a significant part in modulating the mucosal homeostasis. The gut microbiota consists of a large number of microbes of 10^{12} cells/g of the luminal contents, which can be divided into two major bacterial phyla, namely *Bacteroidetes* and *Firmicutes*[17]. Indeed, genetic and epidemiological association have presumed several promising genetic and dietary factors, altering the composition of gut microbiota, in UC[42]. It has been reported that reduction of *Prevotella* and Ruminococcaceae, as well as enrichment of *Streptococcus* and *Enterococcus genera* occurred in adult UC patients[17]. In addition, immunoglobulin A (IgA) is extensively distributed in multiple mucosal layers to exert protective effects against external pathogens. Okai et al.[21] identified the IgA clone W27 displayed the extreme binding ability to various commensal bacteria, while with a weak binding to beneficial bacteria, including *Bifidobacterium bifidum* and *Lactobacillus casei*. As expected, oral administration of W27 IgA could dramatically ameliorate the development of experimental colitis by maintaining the diversity of gut microbiota[21]. Restoration of gut microbiota dysbiosis provides an infusive strategy in preventing and treating UC. In the present study, we indicated that a markedly distinct gut microbial landscape was observed in the normal, vehicle, and apremilast-treated groups (Fig. 6). In keeping with the modulatory effects of apremilast on epithelial barrier function and mucosal immune system, inhibition of PDE4 by apremilast could decrease the relative abundance of colitis-promoting microbes and upregulate the level of beneficial microbes in the gut lumen, which provided further evidence toward the effects of apremilast on mucosal homeostasis. In presence of gut microbiota alteration, the mucosal inflammation and further tissue damage could be rectified following the intervention of PDE4 inhibitor. In accordance, inhibition of PDE4 by apremilast could regulate the antimicrobial responses in the mucus of colon, as evidenced by modulating the tissue-residence of goblet cells, expression of mucins and related genes, including MUC2, CDX2, TFF3, CAMP, and lysozyme (Fig. 7A−G). However, when co-housed with vehicle mice, the therapeutic effects of apremilast on ameliorating mucosal inflammation and tissue damages were largely compromised (Figs. 8 and 9), which indicated that gut microbiota is responsible for apremilast to exert protective effects in chronic UC.

Pathologically, breakdown of the tolerance and defense against commensals and invading pathogens contributes to destroying mucosal barrier function and initiating inflammatory responses in the development of UC[18,34]. Once the intestinal barrier and integrity are impaired, gut PAMPs and DAMPs, including high-mobility group box-1 (HMGB1) and S100 proteins, are exposed and bound to pattern recognition receptors (PPRs)[32]. Fujita et al.[10] found that RNF5, an E3 ubiquitin ligase highly expressing in intestinal epithelial cells, could regulate the stability of its substrate, S100A8, and was decreased along with the development of severe chronic inflammation. Upon inflammatory stimuli, RNF5/S100A8 communication led to activation of colonic DCs and Th1 cells responses[10]. Consistently, administration of neutralization of

S100A8 antibodies displayed therapeutic effects on DSS-induced colitis in *Rnf5*$^{-/-}$ mice, indicating S100 proteins might be the novel therapeutic targets or valuable biomarkers for IBD[10]. It's worth mentioning that S100A8 and S100A9 are principally expressed in monocytes and neutrophils and increased in the presence of inflammatory stimuli in the intestinal epithelial cells. In our study, we found that expression of S100A4, S100A8, S100A9, and S100A10 were increased in the experimental chronic UC (Fig. 7) and TNF-α could induce the overexpression of S100A8 and S100A9 in human epithelial cells, HT-29 (Fig. 7J). While, apremilast could inhibit the expression of S100 proteins both *in vivo* and *in vitro* (Fig. 7).

Over the past decades, accumulating evidence demonstrated that ILCs were widely distributed throughout non-lymphoid and lymphoid organs and functioned as the critical regulators and acquired the pro-inflammatory phenotypes in chronic mucosal inflammation[33,43]. Based on the specific transcription factors, T-bet, GATA3, and RORγt, respectively, ILCs could be divided into three main groups, namely ILC1, ILC2, and ILC3[13]. Previous study showed that *Rag*$^{-/-}$ immunodeficient mice suffered from infection of *Helicobacter hepaticus* could lead to ILC3-mediated chronic UC, which mainly referred to increased expression of IL-17 and IL-23[44]. Interestingly, we found that ILCs in LP, MLNs, and PP were highly increased in colitic mice, along with the overexpression of regulatory factors, including KLRG-1, Eomes, ST2, and NKp46 (Fig. 4F and G), which partially accounted for the dysbiosis of gut microbiota in chronic UC. New data from IBD identified over 24 single nucleotide polymorphisms (SNPs) were closely associated with Th17 intracellular signal transduction and transformation, in which gut microbiota, dietary and energy components, including vitamins A, B3, and D, short chain fatty acid (SFCA), and tryptophan exhibited a central factor in dysfunction of mucosal inflammation[45]. Additionally, attributing to dysfunction of intestinal barrier function, disturbance of gut microbiota, and abnormal expression of integrins and chemokines, the increased populations of innate immune cells, activated NK cells, Th1, Th17 cells were recruited into the mucosal and submucosal layers (Fig. 4A−E). Apremilast exerted effects on reducing the infiltrations of immune cells and attenuated the expression of inflammatory cytokines in the inflamed colons (Fig. S3), which were consistent with the findings that apremilast suppressed the chemotaxis in HT-29 cells and modulated the interaction and communication between epithelial cells and immune cells (Fig. 5G−I). However, when co-housed with vehicle mice, the modulatory effects of apremilast on intestinal mucosal immune activation were largely counteracted (Figs. 8 and 9).

5. Conclusions

Our results demonstrated herein that inhibition of PDE4 by apremilast modulated cAMP-predominant PKA−CREB signaling and ameliorated the clinical symptoms of experimental chronic UC, as evidenced by attenuation of mucosal ulcerations, tissue fibrosis, dysfunction of barrier function, and inflammatory recruitments. Furthermore, we suggested that apremilast could remap the landscape of gut microbiota and rebuilt the mucosal homeostasis by interfering with the cross-talk between human epithelial cells and immune cells. Taken together, the present study revealed that intervene of PDE4 provides an infusive therapeutic strategy for patients with chronic and relapsing UC and is more instrumental for the treatment of UC.

Acknowledgments

This work was granted by the National Science & Technology Major Project "Key New Drug Creation and Manufacturing Program" (2018ZX09711002-006-011, China), Science & Technology Commission of Shanghai Municipality (18431907100, China), CAS Key Laboratory of Receptor Research (SIMM1904YKF-01, China), and "Personalized Medicines-Molecular Signature-based Drug Discovery and Development", Strategic Priority Research Program of the Chinese Academy of Sciences (XDA12020231, China).

Author contributions

Heng Li and Wei Tang designed the research; Heng Li, Chen Fan, Moting Liu, Chunlan Feng, Huimin Lu, Xiaoqian Yang, Qiukai Lu, Caigui Xiang, and Bing Wu performed the experiments. Yao Zhang and Duowu Zou contributed to the collection of human biopsies. Heng Li, Yao Zhang, Duowu Zou, and Wei Tang analyzed the data and wrote the paper. All the authors contributed to the interpretation of data and approved the final draft.

Conflicts of interest

The authors declare no conflicts of interest.

Appendix A. Supporting information

Supporting data to this article can be found online at https://doi.org/10.1016/j.apsb.2021.04.007.

References

1. Li H, Zuo J, Tang W. Phosphodiesterase-4 inhibitors for the treatment of inflammatory diseases. *Front Pharmacol* 2018;**9**:1048.
2. Koga H, Recke A, Vidarsson G, Pas HH, Jonkman MF, Hashimoto T, et al. PDE4 inhibition as potential treatment of epidermolysis bullosa acquisita. *J Invest Dermatol* 2016;**136**:2211−20.
3. Schafer PH, Truzzi F, Parton A, Wu L, Kosek J, Zhang LH, et al. Phosphodiesterase 4 in inflammatory diseases: effects of apremilast in psoriatic blood and in dermal myofibroblasts through the PDE4/CD271 complex. *Cell Signal* 2016;**28**:753−63.
4. Zebda R, Paller AS. Phosphodiesterase 4 inhibitors. *J Am Acad Dermatol* 2018;**78**:S43−52.
5. Kokkonen K, Kass DA. Nanodomain regulation of cardiac cyclic nucleotide signaling by phosphodiesterases. *Annu Rev Pharmacol Toxicol* 2017;**57**:455−79.
6. Parikh K, Antanaviciute A, Fawkner-Corbett D, Jagielowicz M, Aulicino A, Lagerholm C, et al. Colonic epithelial cell diversity in health and inflammatory bowel disease. *Nature* 2019;**567**:49−55.
7. Oshima T, Miwa H. Gastrointestinal mucosal barrier function and diseases. *J Gastroenterol* 2016;**51**:768−78.
8. Neurath MF. Targeting immune cell circuits and trafficking in inflammatory bowel disease. *Nat Immunol* 2019;**20**:970−9.
9. de Souza HSP, Fiocchi C, Iliopoulos D. The ibd interactome: an integrated view of aetiology, pathogenesis and therapy. *Nat Rev Gastroenterol Hepatol* 2017;**14**:739−49.
10. Fujita Y, Khateb A, Li Y, Tinoco R, Zhang T, Bar-Yoseph H, et al. Regulation of S100A8 stability by RNF5 in intestinal epithelial cells determines intestinal inflammation and severity of colitis. *Cell Rep* 2018;**24**:3296−311.e6.
11. Na YR, Stakenborg M, Seok SH, Matteoli G. Macrophages in intestinal inflammation and resolution: a potential therapeutic target in IBD. *Nat Rev Gastroenterol Hepatol* 2019;**16**:531−43.

12. Sharma D, Kanneganti TD. Inflammatory cell death in intestinal pathologies. *Immunol Rev* 2017;**280**:57−73.
13. Sonnenberg GF, Hepworth MR. Functional interactions between innate lymphoid cells and adaptive immunity. *Nat Rev Immunol* 2019;**19**: 599−613.
14. Zeng B, Shi S, Ashworth G, Dong C, Liu J, Xing F. Ilc3 function as a double-edged sword in inflammatory bowel diseases. *Cell Death Dis* 2019;**10**:315.
15. Zundler S, Becker E, Schulze LL, Neurath MF. Immune cell trafficking and retention in inflammatory bowel disease: mechanistic insights and therapeutic advances. *Gut* 2019;**68**:1688−700.
16. Trivedi PJ, Adams DH. Chemokines and chemokine receptors as therapeutic targets in inflammatory bowel disease; pitfalls and promise. *J Crohns Colitis* 2018;**12**:S641−52.
17. McIlroy J, Ianiro G, Mukhopadhya I, Hansen R, Hold GL. Review article: the gut microbiome in inflammatory bowel disease-avenues for microbial management. *Aliment Pharmacol Ther* 2018;**47**:26−42.
18. Rapozo DC, Bernardazzi C, de Souza HS. Diet and microbiota in inflammatory bowel disease: the gut in disharmony. *World J Gastroenterol* 2017;**23**:2124−40.
19. Gao X, Cao Q, Cheng Y, Zhao D, Wang Z, Yang H, et al. Chronic stress promotes colitis by disturbing the gut microbiota and triggering immune system response. *Proc Natl Acad Sci U S A* 2018;**115**: E2960−9.
20. Pigneur B, Sokol H. Fecal microbiota transplantation in inflammatory bowel disease: the quest for the holy grail. *Mucosal Immunol* 2016;**9**: 1360−5.
21. Okai S, Usui F, Ohta M, Mori H, Kurokawa K, Matsumoto S, et al. Intestinal IgA as a modulator of the gut microbiota. *Gut Microb* 2017; **8**:486−92.
22. Danese S, Neurath MF, Kopon A, Zakko SF, Simmons TC, Fogel R, et al. Effects of apremilast, an oral inhibitor of phosphodiesterase 4, in a randomized trial of patients with active ulcerative colitis. *Clin Gastroenterol Hepatol* 2020;**18**:3057.
23. Li H, Fan C, Feng C, Wu Y, Lu H, He P, et al. Inhibition of phosphodiesterase-4 attenuates murine ulcerative colitis through interference with mucosal immunity. *Br J Pharmacol* 2019;**176**: 2209−26.
24. Wirtz S, Popp V, Kindermann M, Gerlach K, Weigmann B, Fichtner-Feigl S, et al. Chemically induced mouse models of acute and chronic intestinal inflammation. *Nat Protoc* 2017;**12**:1295−309.
25. Li H, Fan C, Lu H, Feng C, He P, Yang X, et al. Protective role of berberine on ulcerative colitis through modulating enteric glial cells−intestinal epithelial cells−immune cells interactions. *Acta Pharm Sin B* 2020;**10**:447−61.
26. Huson DH, Mitra S, Ruscheweyh HJ, Weber N, Schuster SC. Integrative analysis of environmental sequences using MEGAN4. *Genome Res* 2011;**21**:1552−60.
27. Xue X, Bredell BX, Anderson ER, Martin A, Mays C, Nagao-Kitamoto H, et al. Quantitative proteomics identifies STEAP4 as a critical regulator of mitochondrial dysfunction linking inflammation and colon cancer. *Proc Natl Acad Sci U S A* 2017; **114**:E9608−17.
28. Li H, Feng C, Fan C, Yang Y, Yang X, Lu H, et al. Intervention of oncostatin M-driven mucosal inflammation by berberine exerts therapeutic property in chronic ulcerative colitis. *Cell Death Dis* 2020;**11**: 271.
29. Pai RK, Jairath V, Vande Casteele N, Rieder F, Parker CE, Lauwers GY. The emerging role of histologic disease activity assessment in ulcerative colitis. *Gastrointest Endosc* 2018;**88**: 887−98.
30. Perez-Aso M, Montesinos MC, Mediero A, Wilder T, Schafer PH, Cronstein B. Apremilast, a novel phosphodiesterase 4 (PDE4) inhibitor, regulates inflammation through multiple camp downstream effectors. *Arthritis Res Ther* 2015;**17**:249.
31. Knoop KA, Newberry RD. Goblet cells: multifaceted players in immunity at mucosal surfaces. *Mucosal Immunol* 2018;**11**:1551−7.
32. Boyapati RK, Rossi AG, Satsangi J, Ho GT. Gut mucosal damps in IBD: from mechanisms to therapeutic implications. *Mucosal Immunol* 2016;**9**:567−82.
33. Pantazi E, Powell N. Group 3 ILCs: peacekeepers or troublemakers? What's your gut telling you?! *Front Immunol* 2019;**10**:676.
34. Cohen LJ, Cho JH, Gevers D, Chu H. Genetic factors and the intestinal microbiome guide development of microbe-based therapies for inflammatory bowel diseases. *Gastroenterology* 2019;**156**: 2174−89.
35. Zhang X, Dong G, Li H, Chen W, Li J, Feng C, et al. Structure-aided identification and optimization of tetrahydro-isoquinolines as novel PDE4 inhibitors leading to discovery of an effective antipsoriasis agent. *J Med Chem* 2019;**62**:5579−93.
36. Raker VK, Becker C, Steinbrink K. The camp pathway as therapeutic target in autoimmune and inflammatory diseases. *Front Immunol* 2016;**7**:123.
37. Li H, Li J, Zhang X, Feng C, Fan C, Yang X, et al. DC591017, a phosphodiesterase-4 (PDE4) inhibitor with robust anti-inflammation through regulating PKA−CREB signaling. *Biochem Pharmacol* 2020; **177**:113958.
38. Bianchi L, Del Duca E, Romanelli M, Saraceno R, Chimenti S, Chiricozzi A. Pharmacodynamic assessment of apremilast for the treatment of moderate-to-severe plaque psoriasis. *Expet Opin Drug Metabol Toxicol* 2016;**12**:1121−8.
39. Huang B, Chen Z, Geng L, Wang J, Liang H, Cao Y, et al. Mucosal profiling of pediatric-onset colitis and ibd reveals common pathogenics and therapeutic pathways. *Cell* 2019;**179**: 1160−76.e24.
40. Lamb CA, O'Byrne S, Keir ME, Butcher EC. Gut-selective integrin-targeted therapies for inflammatory bowel disease. *J Crohns Colitis* 2018;**12**:S653−68.
41. Argollo M, Fiorino G, Hindryckx P, Peyrin-Biroulet L, Danese S. Novel therapeutic targets for inflammatory bowel disease. *J Autoimmun* 2017;**85**:103−16.
42. Khalili H, Chan SSM, Lochhead P, Ananthakrishnan AN, Hart AR, Chan AT. The role of diet in the aetiopathogenesis of inflammatory bowel disease. *Nat Rev Gastroenterol Hepatol* 2018;**15**:525−35.
43. Seo GY, Giles DA, Kronenberg M. The role of innate lymphoid cells in response to microbes at mucosal surfaces. *Mucosal Immunol* 2020;**13**: 399−412.
44. Buonocore S, Ahern PP, Uhlig HH, Ivanov II , Littman DR, Maloy KJ, et al. Innate lymphoid cells drive interleukin-23-dependent innate intestinal pathology. *Nature* 2010;**464**:1371−5.
45. Ueno A, Jeffery L, Kobayashi T, Hibi T, Ghosh S, Jijon H. Th17 plasticity and its relevance to inflammatory bowel disease. *J Autoimmun* 2018;**87**:38−49.